πN and strangeness sigma terms at the physical point with chiral fermions

Yi-Bo Yang,[1] Andrei Alexandru,[2] Terrence Draper,[1] Jian Liang,[1] and Keh-Fei Liu[1]
(χQCD Collaboration)

[1]*Department of Physics and Astronomy, University of Kentucky, Lexington, Kentucky 40506, USA*
[2]*Department of Physics, The George Washington University, Washington, D.C. 20052, USA*
(Received 6 December 2015; published 8 September 2016)

Lattice QCD calculations with chiral fermions of the πN sigma term $\sigma_{\pi N}$ and strangeness sigma term σ_{sN} including chiral interpolation with continuum and volume corrections are provided in this work, with the excited-state contaminations subtracted properly. We calculate the scalar matrix element for the light/strange quark directly and find $\sigma_{\pi N} = 45.9(7.4)(2.8)$ MeV, with the disconnected insertion part contributing 20(12)(4)%, and $\sigma_{sN} = 40.2(11.7)(3.5)$ MeV, which is somewhat smaller than $\sigma_{\pi N}$. The ratio of the strange/light scalar matrix elements is $y = 0.09(3)(1)$.

DOI: 10.1103/PhysRevD.94.054503

I. INTRODUCTION

The πN sigma term $\sigma_{\pi N}$ for the light quark is defined as

$$\sigma_{\pi N} \equiv \hat{m}\langle N|\bar{u}u + \bar{d}d|N\rangle, \tag{1}$$

where $\hat{m} = (m_u + m_d)/2$ is the averaged light quark mass; $|N\rangle$ represents the nucleon state, which is normalized as $\langle N|N\rangle = L^3$ in this case for the unpolarized nucleon at rest; and $\bar{u}u$ and $\bar{d}d$ are the quark bilinear operators. The strangeness sigma term σ_{sN} is similarly defined, with f_s^N being its fraction of the nucleon mass:

$$\sigma_{sN} \equiv m_s\langle N|\bar{s}s|N\rangle, \qquad f_s^N = \frac{\sigma_{sN}}{m_N}. \tag{2}$$

As measures of both explicit and spontaneous chiral symmetry breakings in the baryon sector, $\sigma_{\pi N}$ and σ_{sN} are fundamental quantities which pertain to a wide range of issues in hadron physics, such as the quark mass contribution in the baryon, which is related to the Higgs coupling to observable matter [1–3]; the pattern of $SU(3)$ breaking [2]; πN and KN scatterings [4,5]; and kaon condensate in dense matter [6]. Using a sum rule for the nucleon mass, the heavy quark mass contribution can be deduced from that of the light flavors in the leading order of the strong coupling and the heavy quark limit [1,7]. At the same time, precise values of the quark mass term for various flavors, from light to heavy, are of significant interest for dark matter searches [8–10], where the popular candidates for dark matter (such as the weakly interacting massive particle) interact with the observable world through the Higgs couplings, so that the precise determination of $\sigma_{\pi N}$ and σ_{sN} can provide remarkable constraints on the direct detection of the dark matter candidates.

Phenomenologically, the $\sigma_{\pi N}$ term is typically extracted from the πN scattering amplitude. To the lowest order in m_π^2, the unphysical on-shell isospin-even πN scattering amplitude at the Cheng-Dashen point corresponds to $\sigma(q^2 = 2m_\pi^2)$ [4,5], which can be determined from πN scattering via fixed-q^2 dispersion relation [5]. $\sigma_{\pi N}$ at $q^2 = 0$ can be extracted through a soft correlated two-pion form factor [11–13]. Also, baryon chiral perturbation theory and the Cheng-Dashen theorem have been used to analyze the πN scattering amplitude for $\sigma_{\pi N}(0)$. They give $\sigma_{\pi N}$ values in the range ~45–64 MeV, while the most recent analysis [14] gives 59.1(3.5) MeV.

Both $\sigma_{\pi N}$ and σ_{sN} are amenable to lattice QCD calculations, and there are two ways to calculate them. One is via the Feynman-Hellman theorem, and the other is by directly calculating the matrix elements through the ratio of three-point and two-point correlation functions.

By following the Feynman-Hellman theorem (FH),

$$\sigma_{\pi N} = m_q \left.\frac{\partial m_N(m_q)}{\partial m_q}\right|_{m_q=\hat{m}^{\rm phys}}, \tag{3}$$

where $\hat{m}^{\rm phys}$ is the quark mass corresponding to the physical m_π, one can calculate the nucleon mass at different quark masses and obtain $\sigma_{\pi N}$. A number of such calculations have been performed [15–20], and analyses with chiral extrapolation based on lattice data have also been carried out [2,3,21–23]. Similarly, there have also been a number of direct calculations of $\sigma_{\pi N}$ scalar matrix elements (ME) over the years [24–29], which use Wilson-type fermions that explicitly break chiral symmetry. The most recent three lattice calculations obtained consistent results regardless of whether they used the FH theorem [20] or direct matrix element calculation [28,29], but the common value is around 37(4) MeV and is almost 5σ smaller than the recent phenomenological analysis [14] mentioned above.

Before investigating other avenues to understand the tension between the lattice simulation and phenomenological

analysis [30], a question that cannot be avoided is whether the explicit breaking of chiral symmetry by lattice artifacts, as in the case of Wilson-type fermions, is responsible for the difference. Due to explicit chiral symmetry breaking, the quark mass has an additive renormalization, and the flavor-singlet and nonsinglet quark masses renormalize differently. As a consequence, the strangeness content can be mixed with those of u and d [26,31], leading to a larger value. Attempts have been made to take the flavor mixing into account, which reduce σ_{sN} [26,29,32], with the renormalization factors of the singlet and isovector part of the scalar ME differing by as much as 40% [26].

In contrast, simulations with an overlap fermion for the valence quarks have exact chiral symmetry at finite lattice spacing, and thus they are free of the flavor-mixing problem which afflicts Wilson-type fermions. But the inversion of the chiral fermion is known to be 1 magnitude more expensive than a Wilson-type fermion, which makes the approach numerically challenging. The major task of this work is overcoming the numerical difficulty of addressing the role of chiral symmetry for this quantity. The properties of the overlap action allow us to apply the multimass algorithm to calculate a number of quark masses ranging from the light u/d quark to the strange with little overhead (compared to inversion with one mass). This, together with the use of the low-mode substitution (LMS) technique described in Refs. [1,33], allows us to obtain hundreds of measurements with just a few inversions, thus overcoming the expensive cost of the overlap action required to obtain precise results.

We also present here a direct ME calculation of σ_{sN} without any systematic uncertainty about the flavor mixing of a Wilson-type fermion. As in the case of $\sigma_{\pi N}$, one can take the derivative of the proton mass with respect to the strange quark mass in the sea to get σ_{sN}. But neither the calculations based on the FH theorem [20,34,35] nor phenomenological determinations [2,3,11,23,36] are very precise, since the strange quark dependence of the proton mass is very weak. On the other hand, there are several calculations which use the direct ME calculation [1,26–29,31,37,38]. The present work is the first direct ME calculation with chiral fermions on $(2+1)$-flavor configurations where the pion mass is at the physical point.

In addition to $\sigma_{\pi N}$ and σ_{sN}, the renormalization independent ratio often quoted in the literature,

$$y = \frac{2\langle N|\bar{s}s|N\rangle}{\langle N|\bar{u}u + \bar{d}d|N\rangle}, \tag{4}$$

can be obtained, and it is useful to delineate the $SU(3)$ breaking pattern in the octet baryon spectrum. Its value has not been well determined and the estimates change over time, reflecting the range of uncertainties of $\sigma_{\pi N}$ and σ_{sN}.

Since a precise value of σ_{sN} is hard to obtain from the FH theorem approach, and we want to present both $\sigma_{\pi N}$ and σ_{sN} within the same framework to access the correlation between them, we choose to use the direct ME calculation for both $\sigma_{\pi N}$ and σ_{sN} to obtain the final predictions.

The numerical setup and the details are described in Sec. II. Section III provides our simulation results of $\sigma_{\pi N}$ and σ_{sN}, as well as a comparison with the results from phenomenological analyses and other lattice calculations. This article will be closed by a short summary in Sec. IV.

II. NUMERICAL SETUP

In this work, we use the valence overlap fermions on $(2+1)$-flavor domain-wall fermion (DWF) configurations [39] to carry out the calculation. The effective quark propagator of the massive overlap fermion is the inverse of the operator $(D_c + m)$ [40,41], where D_c is chiral, i.e. $\{D_c, \gamma_5\} = 0$ [42], and its detailed definition can be found in our previous works [1,33,43]. Numerical details regarding the calculation of the overlap operator, eigenmode deflation in inversion of the quark matrix, and the $Z(3)$ grid smeared source with LMS to increase statistics are given in Refs. [1,33,43].

The $(2+1)$-flavor RBC/UKQCD DWF gauge configurations used are on $24^3 \times 64$ (24I), $32^3 \times 64$ (32I) [39] and $48^3 \times 96$ (48I) [44] lattices. Other parameters of the ensembles used are listed in Table I. We used five quark masses from the range $m_\pi \in (250, 400)$ MeV on the first two ensembles, and eight quark masses from $m_\pi \in (114, 400)$ MeV on the last ensemble, which has larger volume and thus allows a lighter pion mass with the constraint $m_\pi L > 3$.

Both the connected and disconnected insertions (CI/DI) contribute to the light quark contents, while the strange sigma term just comes from the disconnected insertion.

The scalar matrix elements are obtained from the ratio of the three-point function to the two-point function:

$$R(t_f, t) = \frac{\langle 0|\int d^3y \Gamma^e \chi(\vec{y}, t_f)\mathcal{O}(t)\sum_{\vec{x}\in G}\overline{\chi}_S(\vec{x}, 0)|0\rangle}{\langle 0|\int d^3y \Gamma^e \chi(\vec{y}, t_f)\sum_{\vec{x}\in G}\overline{\chi}_S(\vec{x}, 0)|0\rangle}, \tag{5}$$

where χ is the standard proton interpolation field and $\overline{\chi}_S$ is the field with Gaussian smearing applied to all three quarks. All the correlation functions from the source points $\vec{x}$ in the grid G are combined to improve the signal-to-noise ratio

TABLE I. The parameters for the RBC/UKQCD configurations [44]: Spatial/temporal size, lattice spacing, residual mass of the DWF sea, the sea strange quark mass under $\overline{\text{MS}}$ scheme at 2 GeV, the pion mass with the degenerate light sea quark (both in units of MeV), and the number of configurations used in this work.

Symbol	$L^3 \times T$	a (fm)	$m_{\text{res}}^{(s)} a$	$m_s^{(s)}$	m_π	N_{cfg}
24I	$24^3 \times 64$	0.1105(3)	0.00315(4)	120	330	203
32I	$32^3 \times 64$	0.0828(3)	0.00067(1)	110	300	309
48I	$48^3 \times 96$	0.1141(2)	0.00061(1)	94.9	139	81

(SNR). $\mathcal{O}(t)$ is the scalar current $\int d^3x\overline{\psi}_f(x,t)\psi_f(x,t)$ located at time slice t and $\Gamma^e = \frac{1}{2}(1+\gamma_4)$. When t_f is large enough, $R(t_f,t)$ is equal to the bare scalar matrix element

$$g_S \equiv \frac{\mathrm{Tr}[\Gamma^e\langle P|\int d^3x\overline{\psi}_f(x)\psi_f(x)|P\rangle]}{\mathrm{Tr}[\Gamma^e\langle P|P\rangle]}, \quad (6)$$

which is t independent, plus t-dependent corrections,

$$R(t_f,t) = g_S + C_1e^{-\Delta E(t_f-t)} + C_2e^{-\Delta Et} + C_3e^{-\Delta Et_f}, \quad (7)$$

where ΔE is the energy difference between the ground state and the first excited state and $C_{1,2,3}$ are the combinations of weights involving the excited states. Then the g_S we want to extract corresponds to the case $0 \ll t \ll t_f$.

For each quark mass on each ensemble, we constructed the ratio $R(t_f,t)$ for three sink-source separations t_f from 0.9 fm to 1.4 fm, and for all the current insertion times t between the source and sink.

A. Connected and disconnected insertion

For the connected insertion, we use the stochastic sandwich method (SSM) with low-mode substitution (LMS) [33] to improve the SNR of the calculation. The stochastic sandwich method uses the stochastic source at the sink time slices to avoid repeating the production of the sequential propagators for different sinks and hadron states, but the final SNR is sensitive to that additional stochastic noise. Our improved stochastic method replaces the long-distance part of the stochastic propagator from the sink to the current by its all-to-all version, using the low-lying eigensystem of D_c, which suppresses the influence of the stochastic noise on the sink propagator.

A regular grid with two smeared sources in each spatial direction for the 24I and 32I lattices (four for the 48I lattice) is placed on two time slices for the 24I and 32I lattices (three for the 48I lattice). The separation between the centers of the neighboring grids in the same time slice is ∼1.3 fm, and each smeared source has a radius of ∼0.5 fm. On the sink side, several noise point-grid sources are placed at three slices t_f which are 0.9–1.4 fm away from the source time slices. Furthermore, the matrix elements of the light scalar contents are dominated by the low-mode part of D_c so that the use of LMS on the propagators from the current to the sink notably reduces the number of noise propagators (from t_f) needed. More details of the stochastic sandwich method with low-mode substitution are given in Ref. [33].

The simulation setup for the connected insertion on three ensembles is listed in Table II. We note that although the 48I ensemble has a larger volume that can accommodate more smeared grid points for the source, which improves the SNR with a single inversion, the SNR around the physical point is still small. So we used five propagators at the source to improve the SNR on the 48I by a factor of 2. The total cost on the 48I ensemble dominates and can be estimated by 34 inversions (with residual 10^{-7}) per configuration. (The cost of the contraction with LMS is about one inversion per source propagator.) The number of ideal equivalent measurements N_{meas} for the grid source at the physical point on the 48I ensemble is 192 (points in grid)×5 (sources) = 960 per configuration and 77,760 in total for the connected insertion.

TABLE II. The source/sink setup on the ensembles, for the connected insertion. N_{grid} is the pattern of the smeared points on a grid source with noise, and N_{src} is the number of propagators with such a source. Three sets of the pair $(\Delta_t^i, N_{\mathrm{sink}}^i)$ are for the sink propagators, with Δ_t^i being the physical distance between the source and sink and N_{sink}^i being the number of noise propagators with such a Δ_t^i.

Ensemble	N_{grid}	N_{src}	Δ_t^1 (fm), N_{sink}^1	Δ_t^2 (fm), N_{sink}^2	Δ_t^3 (fm), N_{sink}^3
24I	$2^3\times 2$	1	0.88, 5	1.11, 5	1.33, 5
32I	$2^3\times 2$	1	0.99, 3	1.16, 3	1.24, 3
48I	$4^3\times 3$	5	0.91, 4	1.14, 8	1.37, 12

The same noise grid-smeared sources are used in the production of the nucleon propagator for the disconnected insertion, and we loop over all the time slices for the nucleon source. The position of the grid is randomly shifted on each time slice. As has been carried out in previous studies of the strangeness content [1] and quark spin [45], the quark loop is calculated with the exact low eigenmodes [low-mode average (LMA)], while the high modes are estimated with eight sets of Z_4 noise on the same (4, 4, 4, 2) grid with odd-even dilution and additional dilution in time. The vacuum expectation value of the quark loops has been subtracted before combining with the proton propagator to get the correlated three-point function.

The fact that the long-distance part of the proton two-point correlation function is dominated by the precise low-lying eigensystem of D_c allows us to use a larger residual of 10^{-4} for the high-mode inversion without affecting the final accuracy. We also used the low-precision inversion with the same residual for the quark loops, since most of the contribution to the disconnected insertion part of g_S comes from the low-mode part of the quark loop, as shown in Fig. 1. So we can treat the quark loop with the scalar insertion as almost being exact. Note that we need four inversions to get a set of the noise propagators: two for different time slices, and two for odd-even dilution for the spatial grid [1].

On the 48I ensemble, the cost of a low-precision (with residual 10^{-4}) inversion is just 1/3 of that for a high-precision inversion (with residual 10^{-7}), and the final cost is equivalent to 37 high-precision inversions per configuration: 32 for the proton propagators with the overhead of LMS, and 5 for the four sets of the noise propagators for the loops. The total number of the measurements of the proton propagator in the ideal case is 4^3 per configuration.

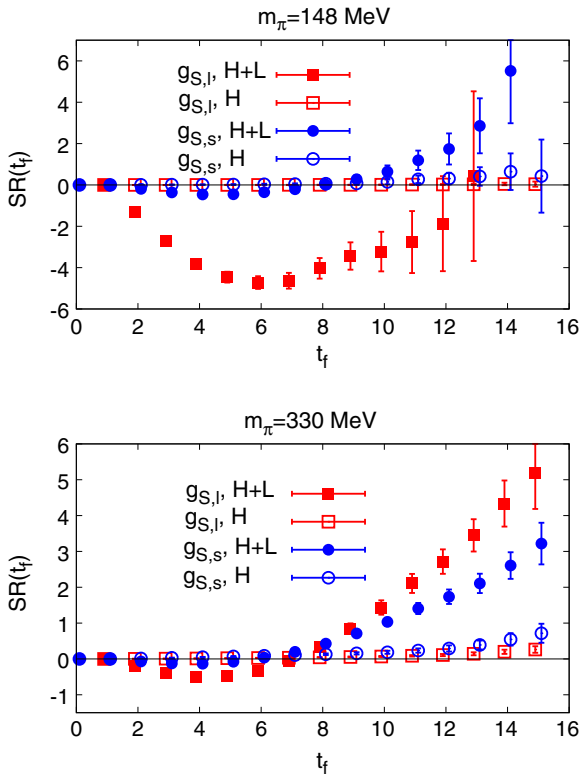

FIG. 1. The light ($m_\pi = 148/330$ MeV in the upper/lower panel respectively) $g_{S,l}$ and strange quark loops $g_{S,s}$, with the quark mass in the nucleon the same as that of the light quark loop, from the 48I lattice are plotted. High-mode contribution (H) and the sum of the high- and low-mode contributions (H + L) to the DI part of the scalar matrix elements are shown separately. The contributions from the stochastic high-mode part of the quark loops are quite small and the results are dominated by the exact low-mode part of the quark loop, so that the LMA method is very effective.

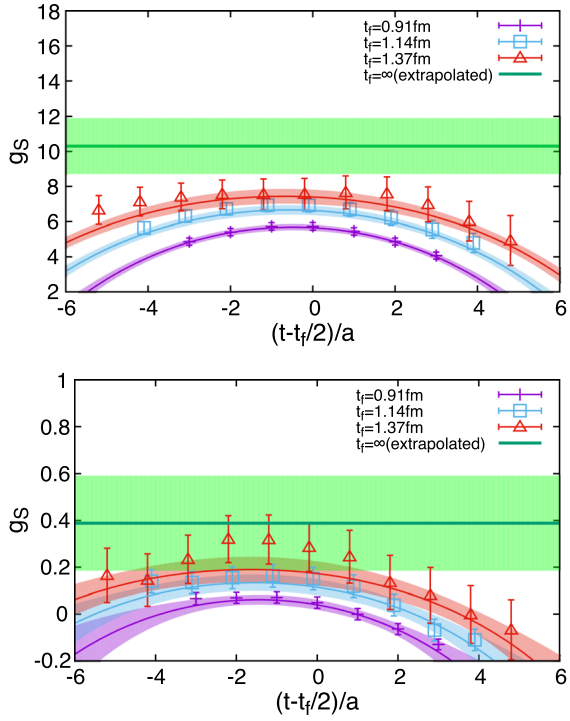

FIG. 2. The ratio $R(t_f, t)$, as a function of the separation t_f (three curves for three separations) and the current position t (the data points on the curves), for each of the light (upper panel) and strange (lower panel) scalar matrix elements in proton, g_S, is plotted at $m_\pi = 148$ MeV (on the 48I ensemble) which is close to the physical point. The green bands show the results extrapolated to infinite separation which correspond to the predictions of g_S. The excited-state contaminations are obvious with the final uncertainties much larger than those for the finite separations.

Therefore, the total number of the measurements of our DI results can be as large as 497,664 in total, if LMS is perfect and all the measurements are independent.

B. Two-state fit

To exclude some excited-state contamination, we dropped the data for which the distance between the current insertion and source (or sink) is smaller than 0.2 fm, and applied the two-state fit in Eq. (7) to obtain the scalar matrix element in the proton for the light quark and also for the strange quark. We show the case of $m_\pi = 148$ MeV on the 48I ensemble in Fig. 2, in which the connected and disconnected insertion parts of the light quark are summed before applying the fit. Note that the curves in Fig. 2 predicted by the fit agree with the data well, and their asymmetry around zero on the horizontal axis is due to the different treatment of source and sink (smeared source and point sink).

In Fig. 3, the ratio $R(t_f, t)$ for $m_\pi \sim 280$ MeV for each of the 24I/32I/48I ensembles is plotted to show the SNR in the relatively heavier pion mass region, and to highlight the qualities of our two-state fit. All curves predicted by the fit agree with the data well, and χ^2/d.o.f. is smaller than 1.4 and the Q value is larger than 0.1, for all the quark masses on all ensembles used in this work.

From the fit, we see that the excited-state contaminations are substantial, and the final prediction of g_S (the green band) is 1σ or 2σ higher than the ratio $R(t_f, t)$ with the largest separation. The error bar on g_S is larger than that on $R(t_f, t)$ at finite separation time t_f due to the extrapolation to infinite t_f.

III. RESULTS

Figure 4 shows the computed $\sigma_{\pi N}$ and σ_{sN} data points for the three ensembles as a function of m_π^2 corresponding to the valence quark mass.

The chiral behavior of $\sigma_{\pi N}$ as a function of m_π can be deduced from the chiral behavior of the nucleon mass itself [as suggested by partially quenched $SU(2)$ χPT [46–48]], by taking the derivative with respect to both valence and sea-quark masses:

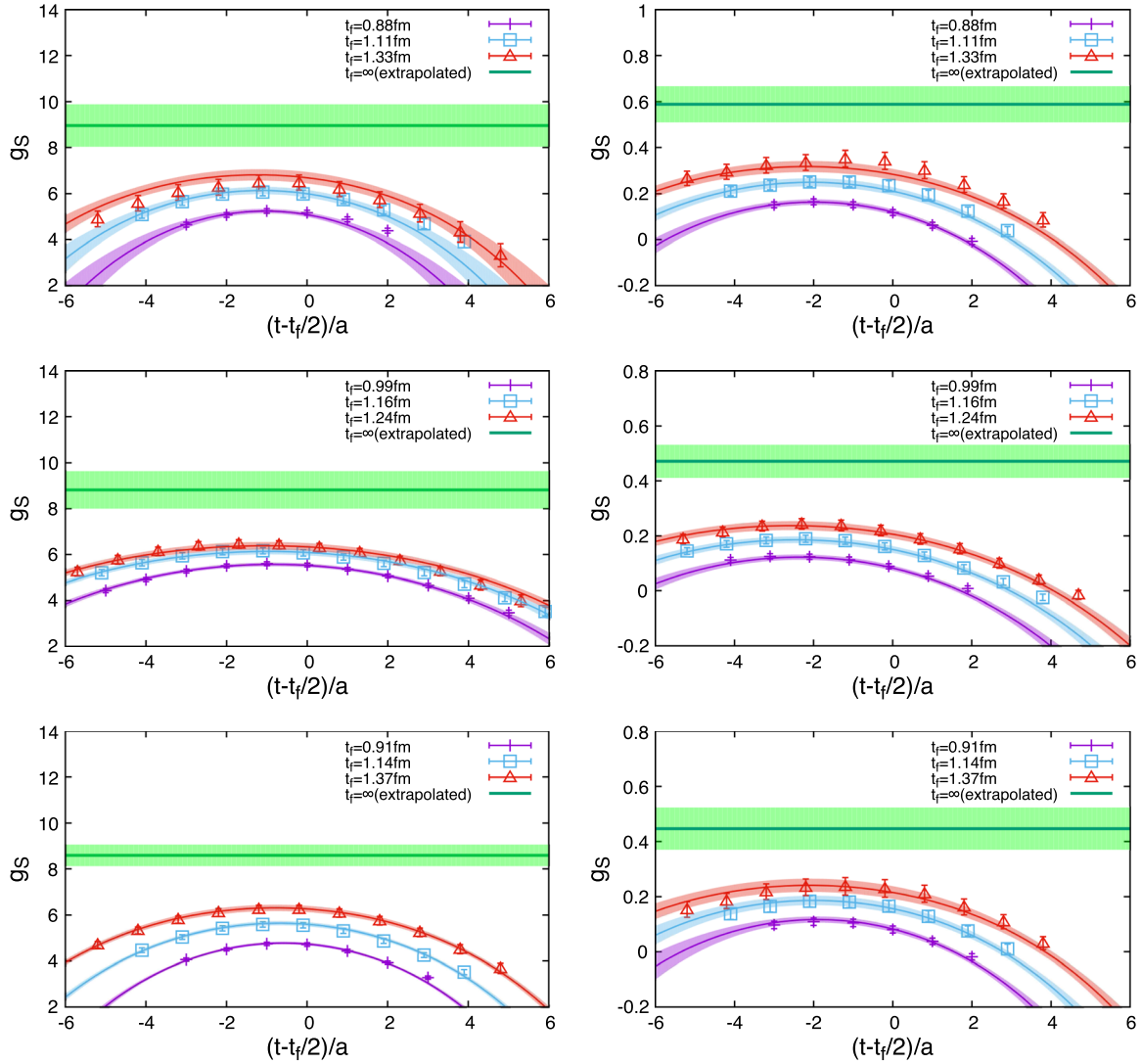

FIG. 3. The ratio $R(t_f, t)$, as a function of the sink-source separation t_f (three curves for three separations) and the current position t (the data points on the curves) for the light and strange matrix elements (left and right panels, respectively). The three sets of the panels from top to bottom show the cases for $m_\pi \sim 280$ MeV on the 24I, 32I, and 48I ensembles, respectively. The green bands show the results extrapolated to infinite separation, which corresponds to the prediction of g_S. The excited-state contaminations are obvious, and the final uncertainties are larger than those on the finite separations.

$$\sigma_{\pi N}(m_l^v, m_l^s, a, L) = C_0^\pi m_{\pi,vv}^2 + C_1^\pi m_{\pi,vv}^3 + C_2^\pi m_{\pi,vs}^2 m_{\pi,vs}^{\rm mix} + C_3^\pi a^2 + C_4^\pi \left(\frac{m_{\pi,vv}^2}{L} - m_{\pi,vv}^3\right) e^{-m_{\pi,vv}L}, \quad (8)$$

with lattice-spacing a and lattice-size L dependence. The symbol $m_{\pi,vv}$ appearing in the above equation is the valence-valence pion mass, and $m_{\pi,vs}^{\rm mix} = \sqrt{m_{\pi,vs}^2 + a^2\Delta_{\rm mix}}$ is the mixed valence sea-pion mass. (The value of $\Delta_{\rm mix}$ in our case is small and contributes a shift of only ~10 MeV to the pion mass at 300 MeV for the 32I lattice [49].)

The chiral log term is dropped, since it can be fully absorbed by the polynomial terms within our present data precision, and will be considered as a systematic uncertainty. Even for the fit of the proton mass itself where a higher precision is attainable, the coefficient of the chiral-log term obtained by Ref. [48] is still consistent with zero with large uncertainty. The functional form of the volume dependence is derived from the leading order of the proton mass [50,51] in χPT.

For σ_{sN}, we used the same functional form for the chiral behavior as in Ref. [1] and added a volume-dependent term

$$\sigma_{sN}(m_l^v, m_l^s, a, L) = C_0^s + C_1^s m_{\pi,vv}^2 + C_2^s m_{\pi,vs}^2 + C_3^s a^2 + C_4^s e^{-m_{\pi,vv}L}. \quad (9)$$

We fit all the data points of $\sigma_{\pi N}$ and σ_{sN} with $m_\pi <$ 350 MeV simultaneously with a correlated fit, with 1000

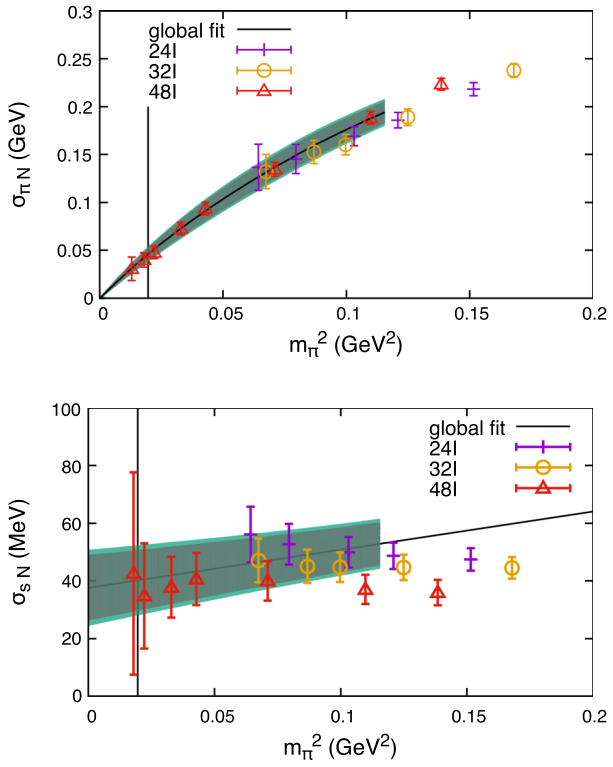

FIG. 4. The summary figures of the light/strange quark content at 18 quark masses on the three ensembles (24I, 32I, and 48I as defined in Table I), as a function of the square of the pion mass. Both the lattice spacing and sea-quark mass dependence are mild. The curve in each figure shows the behavior in the infinite-volume and continuum limits without the partial quenching effect. In each case, the band of the total error is almost the same as that of the statistical error, and thus is barely visible.

TABLE III. The fitted parameters for $\sigma_{\pi N}$ and σ_{sN}. All the parameters are in units of a power of GeV.

$\sigma_{\pi N}$	C_0^π	C_1^π	C_2^π	C_3^π	C_4^π
⋯	2.9(5)	−3.3(1.5)	−0.2(7)	−0.00(3)	47(111)
σ_{sN}	C_0^s	C_1^s	C_2^s	C_3^s	C_4^s
⋯	0.037(13)	0.00(2)	0.13(6)	−0.02(3)	−19(138)

bootstrap resamples on each ensemble, and the final χ^2/d.o.f. is 0.89 with 16 degrees of freedom. The values of the parameters are summarized in Table III. The curves in the infinite volume and continuum limit without the partial quenching effect are plotted in Fig. 4, with bands corresponding to the total error. All the data points stay on that curve within 1 or 2 standard deviations, which means that the finite lattice spacing, sea-quark mass and volume dependences are mild.

We estimate the systematic errors of $\sigma_{\pi N}$ and σ_{sN} as follows:

Discretization errors: We estimate the systematic errors by the differences between the fitting predictions in the continuum limit and those from the ensemble with the smallest lattice spacing (32I).

Finite volume corrections: Similarly, we estimate the systematic errors by the difference between the fitting predictions on the ensemble with the largest volume (48I) and those in the infinite-volume limit.

Chiral extrapolation: The differences between the fitting predictions at the physical pion mass of the 48I ensemble and those from the interpolations of the neighboring quark masses are considered as systematic errors.

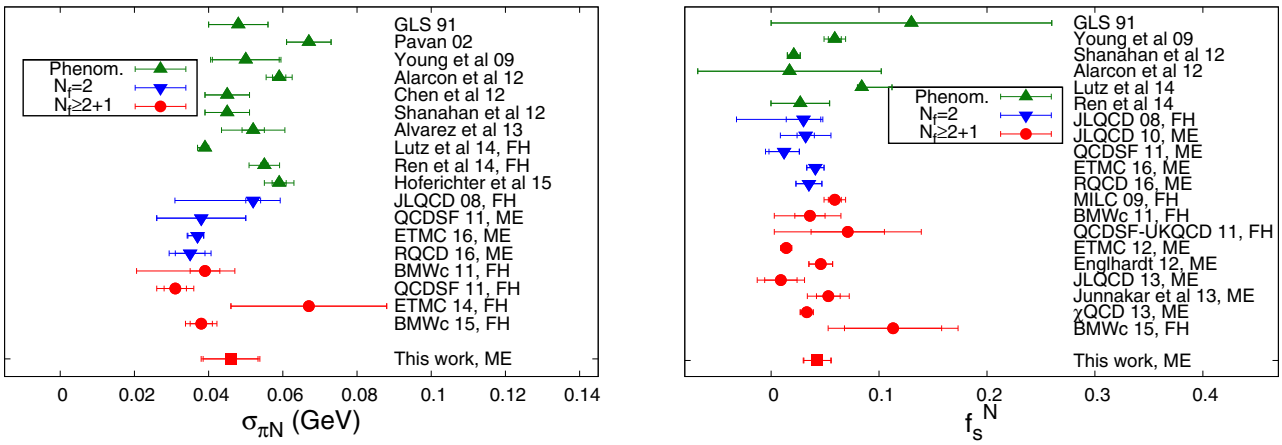

FIG. 5. The results of $\sigma_{\pi N}$ and f_s^N, from both phenomenology and lattice simulations. Numbers are from GLS [11], Pavan [13], Young *et al.* [2], Alarcon *et al.* [36,52], Chen *et al.* [53], Shanahan *et al.* [3], Alvarez *et al.* [21], Lutz *et al.* [22], Ren *et al.* [23], Hoferichter *et al.* [14], JLQCD [15,31,37], QCDSF [26], ETMC [27,28,54], RQCD [29], BMWc [16,20], MILC [34], QCDSF-UKQCD [17], Engelhardt *et al.* [38], Junnarkar *et al.* [35], and χQCD [1]. The narrow error bar for each data point is the statistical error, and the broad bar shows the total uncertainty. The physical proton mass 938 MeV is used to obtain f_s^N in this work.

Strange quark mass: The strange quark mass we used is 101(3)(6) MeV. Since the scalar element will be smaller when the corresponding quark mass is larger, there is just a 1.0 MeV deviation if we change the strange quark mass by 1σ.

Mixed action: We removed the $\Delta_{\rm mix}$ term in the mixed valence sea-pion mass $m^{\rm mix}_{\pi,vs} = \sqrt{m^2_{\pi,vs} + a^2\Delta_{\rm mix}}$ and repeated the fit to simulate the case with the same action for both the valence and sea quark, and the difference turns out to be 2 orders of magnitude smaller than the statistical error.

Chiral log: We added the chiral-log term and repeated the fit for $\sigma_{\pi N}$. The coefficient of the chiral-log term is consistent with zero while the uncertainty of the final prediction increases. The prediction will be changed by 2.2 MeV, and we take this as a systematic uncertainty of $\sigma_{\pi N}$.

The final prediction of $\sigma_{\pi N}$ is 45.9(7.4)(2.8) MeV, where the first error is statistical and the second systematic, as combined in quadrature from those of the continuum and volume extrapolations, chiral and strange quark mass interpolations, the use of the mixed action and dropping the chiral log term. That of σ_{sN} is 40.2(11.7)(3.5) MeV. We determine that the disconnected insertion part contributes 20(12)(4)% of $\sigma_{\pi N}$. We compare our results with other lattice determinations and phenomenological results in Fig. 5.

IV. SUMMARY

We have computed $\sigma_{\pi N}$ and σ_{sN} for 18 quark masses including the physical point on three $(2+1)$-flavor ensembles, including one with the physical pion mass. Since we use chiral fermions in this calculation, there is no additive renormalization of the quark mass for the valence overlap fermion, and $\sigma_{\pi N}$ and σ_{sN} are renormalization group invariant. As a result, there should be no concern about flavor mixing of the scalar matrix elements. A global fit is employed to take into account chiral interpolation, finite lattice spacing, and finite-volume effects. The total uncertainty for $\sigma_{\pi N}$ we achieved is 17%. Our result straddles those of the lattice simulations with Wilson-type fermions and the phenomenological predictions, while none of them can be excluded by our present uncertainty. More precise measurements for the disconnected insertion part are required to make a clear adjudication.

The error of σ_{sN} is somewhat larger than the former estimate of our collaboration [40(12) MeV versus 33(6) MeV] [1], mostly due to a better control of the excited-state contamination. Even so, it is still the most precise result among $(2+1)$-flavor lattice calculations today which include all the systematic uncertainties. Our results show that the contributions from the quark mass of the two light flavors and that from the strange flavor are close to each other. Based on the values of $\sigma_{\pi N}$ and σ_{sN}, we obtain the ratio $y = 0.09(3)(1)$.

ACKNOWLEDGMENTS

We thank the RBC and UKQCD collaborations for providing us their DWF gauge configurations. This work is supported in part by U.S. DOE Grant No. DE-SC0013065. A. A. is supported in part by National Science Foundation CAREER Grant No. PHY-1151648 and by U.S. DOE Grant No. DE-FG02-95ER40907. Y. Y. also thanks the Department of Energy's Institute for Nuclear Theory at the University of Washington for its partial support and hospitality. This research used resources of the Oak Ridge Leadership Computing Facility at the Oak Ridge National Laboratory, which is supported by the Office of Science of the U.S. Department of Energy under Contract No. DE-AC05-00OR22725.

[1] M. Gong *et al.* (χQCD Collaboration), Phys. Rev. D **88**, 014503 (2013).
[2] R. D. Young and A. W. Thomas, Phys. Rev. D **81**, 014503 (2010).
[3] P. E. Shanahan, A. W. Thomas, and R. D. Young, Phys. Rev. D **87**, 074503 (2013).
[4] L. S. Brown, W. J. Pardee, and R. D. Peccei, Phys. Rev. D **4**, 2801 (1971).
[5] T. P. Cheng and R. F. Dashen, Phys. Rev. D **4**, 1561 (1971).
[6] D. B. Kaplan and A. E. Nelson, Phys. Lett. B **175**, 57 (1986).
[7] M. A. Shifman, A. I. Vainshtein, and V. I. Zakharov, Phys. Lett. **78B**, 443 (1978).
[8] T. Falk, A. Ferstl, and K. A. Olive, Phys. Rev. D **59**, 055009 (1999); **60**, 119904(E) (1999).
[9] J. R. Ellis, K. A. Olive, and C. Savage, Phys. Rev. D **77**, 065026 (2008).
[10] J. Giedt, A. W. Thomas, and R. D. Young, Phys. Rev. Lett. **103**, 201802 (2009).
[11] J. Gasser, H. Leutwyler, and M. E. Sainio, Phys. Lett. B **253**, 252 (1991).
[12] T. Becher and H. Leutwyler, Eur. Phys. J. C **9**, 643 (1999).
[13] M. M. Pavan, I. I. Strakovsky, R. L. Workman, and R. A. Arndt, PiN Newslett. **16**, 110 (2002).
[14] M. Hoferichter, J. Ruiz de Elvira, B. Kubis, and U.-G. Meißner, Phys. Rev. Lett. **115**, 092301 (2015).

[15] H. Ohki, H. Fukaya, S. Hashimoto, H. Matsufuru, J. Noaki, T. Onogi, E. Shintani, and N. Yamada (JLQCD Collaboration), *Proc. Sci.*, LATTICE2008 (2008) 126.
[16] S. Durr *et al.*, Phys. Rev. D **85**, 014509 (2012); **93**, 039905 (E) (2016).
[17] R. Horsley, Y. Nakamura, H. Perlt, D. Pleiter, P. E. L. Rakow, G. Schierholz, A. Schiller, H. Stuben, F. Winter, and J. M. Zanotti (QCDSF-UKQCD), Phys. Rev. D **85**, 034506 (2012).
[18] C. Alexandrou, V. Drach, K. Jansen, C. Kallidonis, and G. Koutsou, Phys. Rev. D **90**, 074501 (2014).
[19] G. S. Bali *et al.*, Nucl. Phys. **B866**, 1 (2013).
[20] S. Durr *et al.*, Phys. Rev. Lett. **116**, 172001 (2016).
[21] L. Alvarez-Ruso, T. Ledwig, J. Martin Camalich, and M. J. Vicente-Vacas, Phys. Rev. D **88**, 054507 (2013).
[22] M. F. M. Lutz, R. Bavontaweepanya, C. Kobdaj, and K. Schwarz, Phys. Rev. D **90**, 054505 (2014).
[23] X.-L. Ren, L.-S. Geng, and J. Meng, Phys. Rev. D **91**, 051502 (2015).
[24] S. J. Dong, J. F. Lagae, and K. F. Liu, Phys. Rev. D **54**, 5496 (1996).
[25] M. Fukugita, Y. Kuramashi, M. Okawa, and A. Ukawa, Phys. Rev. D **51**, 5319 (1995).
[26] G. S. Bali *et al.* (QCDSF Collaboration), Phys. Rev. D **85**, 054502 (2012).
[27] S. Dinter, V. Drach, R. Frezzotti, G. Herdoiza, K. Jansen, and G. Rossi (ETM Collaboration), J. High Energy Phys. 08 (2012) 037.
[28] A. Abdel-Rehim, C. Alexandrou, M. Constantinou, K. Hadjiyiannakou, K. Jansen, C. Kallidonis, G. Koutsou, and A. V. Aviles-Casco (ETM Collaboration), Phys. Rev. Lett. **116**, 252001 (2016).
[29] G. S. Bali, S. Collins, D. Richtmann, A. Schäfer, W. Söldner, and A. Sternbeck (RQCD Collaboration), Phys. Rev. D **93**, 094504 (2016).
[30] M. Hoferichter, J. R. de Elvira, B. Kubis, and U.-G. Meißner, Phys. Lett. B **760**, 74 (2016).
[31] K. Takeda, S. Aoki, S. Hashimoto, T. Kaneko, J. Noaki, and T. Onogi (JLQCD Collaboration), Phys. Rev. D **83**, 114506 (2011).
[32] C. Michael, C. McNeile, and D. Hepburn (UKQCD Collaboration), Nucl. Phys. B, Proc. Suppl. **106**, 293 (2002).
[33] Y.-B. Yang, A. Alexandru, T. Draper, M. Gong, and K.-F. Liu, Phys. Rev. D **93**, 034503 (2016).
[34] D. Toussaint and W. Freeman (MILC Collaboration), Phys. Rev. Lett. **103**, 122002 (2009).
[35] P. Junnarkar and A. Walker-Loud, Phys. Rev. D **87**, 114510 (2013).
[36] J. M. Alarcon, L. S. Geng, J. Martin Camalich, and J. A. Oller, Phys. Lett. B **730**, 342 (2014).
[37] H. Ohki, K. Takeda, S. Aoki, S. Hashimoto, T. Kaneko, H. Matsufuru, J. Noaki, and T. Onogi (JLQCD Collaboration), Phys. Rev. D **87**, 034509 (2013).
[38] M. Engelhardt, Phys. Rev. D **86**, 114510 (2012).
[39] Y. Aoki *et al.* (RBC, UKQCD collaborations), Phys. Rev. D **83**, 074508 (2011).
[40] T.-W. Chiu, Phys. Rev. D **60**, 034503 (1999).
[41] K.-F. Liu, Int. J. Mod. Phys. A **20**, 7241 (2005).
[42] T.-W. Chiu and S. V. Zenkin, Phys. Rev. D **59**, 074501 (1999).
[43] A. Li *et al.* (χQCD Collaboration), Phys. Rev. D **82**, 114501 (2010).
[44] T. Blum *et al.* (RBC, UKQCD collaborations), Phys. Rev. D **93**, 074505 (2016).
[45] M. Gong, Y.-B. Yang, A. Alexandru, T. Draper, and K.-F. Liu, arXiv:1511.03671.
[46] S. R. Beane and M. J. Savage, Nucl. Phys. **A709**, 319 (2002).
[47] B. C. Tiburzi, Phys. Rev. D **72**, 094501 (2005); **79**, 039904(E) (2009).
[48] A. Walker-Loud *et al.*, Phys. Rev. D **79**, 054502 (2009).
[49] M. Lujan, A. Alexandru, Y. Chen, T. Draper, W. Freeman, M. Gong, F. X. Lee, A. Li, K. F. Liu, and N. Mathur, Phys. Rev. D **86**, 014501 (2012).
[50] A. Ali Khan *et al.* (QCDSF-UKQCD), Nucl. Phys. **B689**, 175 (2004).
[51] S. R. Beane, Phys. Rev. D **70**, 034507 (2004).
[52] J. M. Alarcon, J. Martin Camalich, and J. A. Oller, Phys. Rev. D **85**, 051503 (2012).
[53] Y.-H. Chen, D.-L. Yao, and H. Q. Zheng, Phys. Rev. D **87**, 054019 (2013).
[54] C. Alexandrou, S. Dinter, V. Drach, K. Jansen, K. Hadjiyiannakou, and D. B. Renner (ETM Collaboration), Eur. Phys. J. C **74**, 2692 (2014).